



DGAT2 partially compensates for lipid-induced ER stress in human DGAT1-deficient intestinal stem cells^S

Jorik M. van Rijn,^{*,†} Marliek van Hoesel,^{*,†} Cecilia de Heus,[§] Anke H. M. van Vugt,^{*,†} Judith Klumperman,[§] Edward E. S. Nieuwenhuis,^{*} Roderick H. J. Houwen,^{*} and Sabine Middendorp^{1,*,†}

Division of Pediatrics, Department of Pediatric Gastroenterology, Wilhelmina Children's Hospital,^{*} Regenerative Medicine Center,[†] and Department of Cell Biology, Center for Molecular Medicine,[§] University Medical Center Utrecht, Utrecht University, Utrecht, The Netherlands

ORCID IDs: 0000-0003-2865-4455 (J.M.v.R.); 0000-0002-0925-0095 (S.M.)

Abstract Dietary lipids are taken up as FAs by the intestinal epithelium and converted by diacylglycerol acyltransferase (DGAT) enzymes into triglycerides, which are packaged in chylomicrons or stored in cytoplasmic lipid droplets (LDs). DGAT1-deficient patients suffer from vomiting, diarrhea, and protein losing enteropathy, illustrating the importance of this process to intestinal homeostasis. Previously, we have shown that DGAT1 deficiency causes decreased LD formation and resistance to unsaturated FA lipotoxicity in patient-derived intestinal organoids. However, LD formation was not completely abolished in patient-derived organoids, suggesting the presence of an alternative mechanism for LD formation. Here, we show an unexpected role for DGAT2 in lipid metabolism, as DGAT2 partially compensates for LD formation and lipotoxicity in DGAT1-deficient intestinal stem cells. Furthermore, we show that (un)saturated FA-induced lipotoxicity is mediated by ER stress.¹ More importantly, we demonstrate that overexpression of DGAT2 fully compensates for the loss of DGAT1 in organoids, indicating that induced DGAT2 expression in patient cells may serve as a therapeutic target in the future.—van Rijn, J. M., M. van Hoesel, C. de Heus, § A. H. M. van Vugt, J. Klumperman, E. E. S. Nieuwenhuis, R. H. J. Houwen, and S. Middendorp. **DGAT2 partially compensates for lipid-induced ER stress in human DGAT1-deficient intestinal stem cells.** *J. Lipid Res.* 2019. 60: 1787–1800.

Supplementary key words intestine • triglycerides • diet and dietary lipids • diseases • fatty acid • lipid droplets • lipotoxicity • diacylglycerol acyltransferase 2 • diacylglycerol acyltransferase 1

Interest in the systemic response to dietary lipids has gained attention, as the global spread of a Western lifestyle has led to a vast increase in the occurrence of obesity (1). This trend has a significant impact on global healthcare, as

obesity is strongly correlated with an increased risk of a wide variety of health problems, including diabetes, heart disease, and colorectal cancer (2, 3). Although much research has focused on the systemic effects of a high-fat diet (HFD), much remains unknown about how the intestinal epithelium copes with lipid-induced stress as the primary port of entry for dietary lipids.

Lipids in the human diet consist mainly of triglycerides (TGs), which comprise a mixture of saturated FAs (SFAs) and unsaturated FAs (UFAs). In the intestine, these hydrophobic TGs are emulsified and subsequently hydrolyzed by lipases into monoglycerides and FFAs. Diacylglycerol acyltransferase (DGAT)1, located on the ER, finally catalyzes the synthesis of TG from fatty acyl-CoA and diacylglycerol (DG). The resulting hydrophobic TGs are either packaged in chylomicrons (CMs) for export into the lymph or stored in cytosolic lipid droplets (LDs) (4). Interest in this process has increased in the last decade because the intestine has been found to store dietary lipids locally for delayed release up to 16 h post-meal (5). The intestine is therefore potentially an important regulating organ for systemic lipid metabolism, instead of solely a port of entry. Furthermore, it has been shown in other cell types, including murine fibroblasts and adipocytes, that DGAT1 is involved in the

Abbreviations: CHOP, C/EBP homologous protein; CM, chylomicron; DG, diacylglycerol; DGAT, diacylglycerol acyltransferase; D1i, diacylglycerol acyltransferase 1 inhibitor; D2i, diacylglycerol acyltransferase 2 inhibitor; D2OE, DGAT2 overexpression; DM, differentiation medium; EM, expansion medium; HFD, high-fat diet; IRE1, inositol requiring enzyme 1; LC₅₀, concentration resulting in half-maximal cell lethality; LD, lipid droplet; MFI, mean fluorescent intensity; OA, oleic acid; PA, palmitic acid; PERK, RNA-activated protein kinase-like ER kinase; PI, propidium iodide; PLE, protein losing enteropathy; SFA, saturated FA; SSC-A, side scatter area; TG, triglyceride/triacylglycerol; UFA, unsaturated FA; UPR, unfolded protein response; XBP1, X-box binding protein 1.

¹To whom correspondence should be addressed.

e-mail: s.middendorp@umcutrecht.nl

^S The online version of this article (available at <http://www.jlr.org>) contains a supplement.

This work was supported by Netherlands Organisation for Scientific Research (NWO-ZonMW-VIDI) Grant 016.146.353 (to S.M.).

Manuscript received 26 March 2019 and in revised form 17 July 2019.

Published, JLR Papers in Press, July 17, 2019

DOI <https://doi.org/10.1194/jlr.M094201>

Copyright © 2019 van Rijn et al. Published under exclusive license by The American Society for Biochemistry and Molecular Biology, Inc.

This article is available online at <http://www.jlr.org>

formation of LDs, which protect these tissues from lipid-induced stress upon high FA load (6–9).

Recently, we have shown that patients deficient for DGAT1 have severe clinical features, such as protein losing enteropathy (PLE), vomiting and/or diarrhea, fat intolerance, and failure to thrive due to impaired fat metabolism, but fare well on a lipid-restricted diet (10). As PLE in combination with diarrhea can be the result of mucosal injury in the intestine (11), the concurrent fat intolerance indicated that DGAT1 protects the epithelium from lipid-induced damage. By using patient-derived dermal fibroblasts and intestinal organoids, we have shown that DGAT1 mediates LD formation, and DGAT1 deficiency increases sensitivity to lipid-induced toxicity and apoptosis of intestinal epithelial cells. However, LD formation was not completely abolished in patient-derived DGAT1-deficient cells upon stimulation with the most common UFA, oleic acid (OA) (10). So far, it was not resolved how LD formation was established in the absence of DGAT1, or by what mechanism LD formation protects the epithelium against lipotoxicity. The availability of patient-derived intestinal organoids provides a unique opportunity to study LD-mediated protection against lipotoxicity specifically in human intestinal epithelial cells.

The DGAT1-independent LD forming capacity we found in patient-derived intestinal organoids hints toward the presence of an endogenous rescue mechanism, and therefore to a potential target for treatment of DGAT1-deficient patients. As DGAT2, an isozyme of DGAT1, was previously described to contribute to LD formation in other cell types and organisms (12–14), we hypothesized that the DGAT1-independent LD formation we have observed previously was mediated by DGAT2 activity.

Here, we determined whether DGAT2 has a role in LD formation and by which mechanism lipid-induced cytotoxicity is mediated in DGAT1-deficient intestinal organoids. As such, we determined the effects of both DGAT1- and DGAT2-mediated lipid metabolism on the homeostasis of the intestinal epithelium. We show that epithelial stem cells express both functional DGAT1 and DGAT2, despite the fact that DGAT2 was previously shown to be expressed only in very low levels in human intestine (15, 16). Furthermore, we show that functional DGAT2 expression is lost upon differentiation toward an enterocyte phenotype, and DGAT2 can partially compensate for LD formation and resistance to lipotoxicity when DGAT1 function is inhibited in intestinal stem cells. In addition, we show that DGAT1-dependent OA-induced LD formation is required for tolerance to the SFA, palmitic acid (PA), in human intestinal stem cells, which was also partially dependent on DGAT2 in the absence of DGAT1. Furthermore, we link the protective effect of LDs to diminished lipid-induced ER stress. Finally, we show that overexpression of DGAT2 fully rescued OA-mediated lipotoxicity in patient-derived DGAT1-deficient intestinal cells.

Together, our data indicate that DGAT enzymes are of crucial importance to protect the intestine from toxic concentrations of FAs. Furthermore, our results indicate that DGAT2 could have a functional role in the human

intestinal stem cell niche and may serve as a therapeutic target to treat diseases related to intestinal lipid uptake.

MATERIALS AND METHODS

Study approval

This study was approved by the responsible local ethics committee (Institutional Review Board of the University Medical Center Utrecht). All participants provided written informed consent for the collection of samples and subsequent analysis. The study was conducted in accordance with the ethical principles set forth in the Declaration of Helsinki.

Human subject details

All organoid cultures were derived from duodenal intestinal biopsies. The control and patient groups were each made up of three individuals, referred to as control or patient 1, 2, or 3. Control 1 was a 4-year-old male at the time the biopsy was taken, control 2 a 4-year-old female, and control 3 a 9-year-old female. Extensive clinical details for each patient are provided in (10), where patients 1, 2, and 3 in this study are referred to as patients 7, 8, and 9, respectively, in our previous study. Patients 1 and 2 are brothers from a consanguineous Dutch family, respectively 12 and 15 years old at the time the biopsy was taken. Patient 3 was a 9-year-old female from a Dutch family of unknown consanguinity and sister of a monozygotic twin pair.

The human SI epithelium control used for Western blot was isolated from an ileum resection from a newborn male infant.

Culture and differentiation of human intestinal organoids

Crypts were isolated from biopsies as described previously (17, 18) and grown into organoids as described previously (10). In short, crypts were isolated from intestinal biopsies by dissociation with 10 mM EDTA in PBS and collected by pipetting vigorously. Isolated crypts were resuspended in growth factor-free medium, consisting of Advanced DMEM/F12 (Gibco), 100 U/ml penicillin-streptomycin (Gibco), 10 mM HEPES (Gibco), and GlutaMAX (Gibco). Matrigel (Corning) was added to a final concentration of 70% and plated on prewarmed cell culture 24- or 96-well plates. After Matrigel polymerization, organoid culture medium (hSI-EM) was added consisting of growth factor-free medium, 50% WNT3A-conditioned medium, 20% R-spondin-1-conditioned medium, 10% Noggin-conditioned medium, 50 ng/ml murine EGF (Peprotech, London, UK), 10 mM nicotinamide (Sigma-Aldrich), 1.25 mM N-acetyl (Sigma-Aldrich), B27 (Gibco), 500 nM TGF- β inhibitor A83-01 (Tocris, Bristol, UK), 10 μ M P38 inhibitor SB202190 (Sigma-Aldrich). Organoids were cultured at 37°C and 5% CO₂, and medium was refreshed every 2–3 days. The organoids were passaged as single cells using TrypLE Express (Thermo Fisher Scientific), counted, and seeded as 250 cells/ μ l in the Matrigel mix. After passaging, 10 μ M Rho-associated coiled-coil containing protein kinase (ROCK) inhibitor Y-27632 (Abcam, Cambridge, UK) was added for the first 2–3 days of the culture. To induce differentiation, organoids were cultured in differentiation medium (hSI-DM) for 5 days, which consists of hSI-EM lacking WNT3A-conditioned medium, nicotinamide, and SB202190.

LD assays

The LD assays were performed as described previously (10). In short, OA-BSA conjugate was prepared by heating 0.2 g OA (Sigma-Aldrich) to 70°C in 1.5 ml PBS. The OA suspension was then thoroughly vortexed and slowly added to a solution of FA-free BSA (Sigma-Aldrich) in PBS kept at 37°C in a molar ratio of OA:BSA (8:1) to a final stock concentration of 20 mM OA and 2.5

mM BSA. PA (Sigma-Aldrich) was first saponified to 100 mM in 0.1 M NaOH and kept at 70°C for 1 h before conjugation to BSA in a final stock concentration of 10 mM in an 8:1 ratio as described for OA. Organoids were grown in expansion medium (EM) on tissue culture-treated 96-well plates. After 5 days of EM or 5 days of differentiation on differentiation medium (DM), the organoids were incubated with FA-BSA for 17 h in the presence or absence of 0.1 μ M DGAT1 inhibitor (D1i) (AZD 3988; Tocris) for EM, 1 μ M D1i for DM, and/or 14 nM DGAT2 inhibitor (D2i) (PF-06424439; Sigma-Aldrich). Organoids were then fixed in 4% formaldehyde for 30 min at room temperature. Cells were washed in PBS and stained with 0.025 mg/ml LD540 and DAPI (Sigma-Aldrich) in PBS for 15 min at room temperature in the dark. Cells were washed and stored in PBS. Imaging of the organoids was performed using a Leica SP8X laser-scanning confocal microscope outfitted with a white light laser. The acquired stacks were processed and analyzed with Fiji/ImageJ (19, 20); shown are maximum projections of approximately 10 micron stacks.

For the flow cytometric analysis, organoids were grown and treated with OA-BSA in the same manner as for the confocal analysis. After incubation with OA-BSA, the cells were harvested by pipetting and dissociated using TrypLE Express (Thermo Fisher) until single cells were acquired. The cells were then fixed and stained in the same manner as for the confocal analysis and assayed using a BD FACS Canto II. The results were analyzed using FlowJo® software and statistical analysis was performed using GraphPad Prism 7 software.

Western blot

Organoids were lysed in Laemmli buffer [0.12 M Tris-HCl (pH 6.8), 4% SDS, 20% glycerol, 0.05 g/l bromophenol blue, 35 mM β -mercaptoethanol] and incubated at 100°C for 5 min. Human ileum resection material was gently scraped with a scalpel and used as the ex vivo control sample. The protein concentration was measured using a BCA assay. Equal amounts of protein were separated by SDS-PAGE on a 12% acrylamide gel and transferred to a polyvinylidene difluoride membrane using a Trans-Blot® Turbo according to manufacturer's protocol. The membrane was then blocked with 5% milk protein in TBST [0.3% Tween, 10 mM Tris-HCl (pH 8), and 150 mM NaCl in distilled water] and probed with primary antibodies. The membranes were washed with TBST and incubated with appropriate secondary antibodies. Immunocomplexes were detected using the LI-COR Odyssey.

The primary antibodies used were rabbit anti-DGAT1 (1:1,000, ab181180; Abcam), rabbit anti-DGAT2 (1:1,000, bs-12998R; Bioss Antibodies), mouse anti-ACTB (sc-47778; Santa Cruz Biotechnology). The secondary antibodies used were donkey anti-rabbit IgG IRDye 680 (1:20,000, 926-32222; LI-COR) and donkey anti-mouse IgG IRDye 800RD (1:20,000, 926-32222; LI-COR). Band intensities were quantified using Fiji/ImageJ. Within lanes, band intensities for DGAT1 and DGAT2 were normalized to ACTB.

Quantitative real-time PCR

RNA was isolated using TRIzol® LS reagent (Thermo Fisher) from organoids grown in either EM for 10 days or EM for 5 days and subsequently DM for 5 days according to the manufacturer's protocol. cDNA was synthesized using the iScript cDNA synthesis kit (Bio-Rad) and amplified using SYBR green supermix (Bio-Rad) in a Light Cycler96® (Bio-Rad) according to the manufacturer's protocol. The comparative Ct method was used to quantify the data. The relative quantity was defined as $2^{-\Delta\Delta C_t}$. Primers are listed in supplemental Table S3, HP1BP3 was used as housekeeper gene. For quantification of (un)spliced X-box binding protein 1 (XBP1), we performed a PCR for XBP1 using GoTaq® DNA polymerase (Promega) and Green GoTaq® Flexi buffer (Promega) with 20 ng template according to the manufacturer's protocol. The PCR was performed on a Bio-Rad T100 Thermo Cycler at

62°C for 30 cycles, the product run on a 1% agarose gel, and visualized using SYBR Safe DNA Gel stain (Thermo Fisher).

Transmission electron microscopy

Intestine organoids of patient cells and healthy control cells were fixed at room temperature by adding Karnovsky fixative [2.5% glutaraldehyde and 2% formaldehyde (Electron Microscopy Sciences) in 0.1 M phosphate buffer (pH 7.4)] 1:1 to the cell culture medium for 10 min. This was replaced by fresh fixative solution and incubated for 2 h at room temperature. Cells were then postfixed for 2 h at 4°C with 1% OsO₄/1.5% K₃Fe(III)(CN)₆ in 0.065 M phosphate buffer and finally 1 h with 0.5% uranyl acetate in demi water. After fixation, cells were dehydrated and embedded in Epon epoxy resin (Polysciences). Ultrathin sections of 60 nm were contrasted with uranyl acetate and lead citrate using the AC20 (Leica) and examined with a T12 electron microscope (Thermo Fisher). Images were collected from three control and three patient organoid lines per experimental condition.

All the measurements were done using ImageJ. LD number and area quantification was done using the freehand tool. This was done for 20 cells per sample and a total of 60 cells per condition. This dataset was cleaned using R, where “null” measurements for the LD area were removed. Subsequently, the average number of LDs per cell was calculated for 60 cells per condition, and statistical analysis was performed with an unpaired *t*-test using GraphPad Prism. The size of individual LDs was presented as a density plot using the ggplot2 package for R.

Propidium iodide lipotoxicity assay

The organoid lipotoxicity assays were performed as described previously (10). Briefly, for the propidium iodide (PI) staining, organoids were grown and incubated with varying concentrations of FA as described for the LD confocal assay. The organoids were then stained with Hoechst 33342 (1 μ g/ml) (Sigma-Aldrich) and PI (0.1 mg/ml) (Thermo Fisher) in DMEM without phenol red (Gibco) at room temperature for 15 min. Organoids were imaged using a Zeiss LSM800 confocal microscope. Resulting images were analyzed using Fiji/ImageJ (19, 20) for the total area of fluorescence of PI. To calculate the percentage of maximum assay response, the total area of PI fluorescence was normalized to the total live and dead cell signal per well according to the formula $R_x = P_x / (P_x + H_x)$ where *P* is the total area of PI fluorescence and *H* the total area of Hoechst fluorescence for FA concentration *x*, where *x* ranges [0, ..., *n*]. Then, the percentage of maximum assay response was calculated as $(R_x - R_0) / [\max(R_x) - R_0] \times 100\%$. The resulting percentage of total area response was averaged across technical duplicates for each line of intestinal organoids, and three biological replicates were included in the groups control and patient. Percentages of total assay response for the three biological replicates were plotted against the log₁₀([FA]) using GraphPad Prism and fitted with a nonlinear regression with variable slope. Where applicable, the concentration resulting in half-maximal cell lethality (LC₅₀) is defined as $10^{\log_{10}([FA])}$, giving the concentration of FA where 50% of total assay response is reached. In Tables 1 and 2, values are reported as LC₅₀ = mean [95% CI].

Lentiviral DGAT2 overexpression

DGAT2 overexpressing (D2OE) intestinal organoids were generated by transduction with a lentiviral overexpression construct. A lentiviral vector was constructed by cloning the DGAT2 complementary sequence from HEK293T cDNA with primers containing *Age*I and *Xba*I restriction sites and subsequent T4 ligation into the pLenti-CMV-GFP-Hygro plasmid (21) (supplemental Fig. S5). The DGAT2 stop-codon was kept in this construct, and thus it does not produce a GFP fusion protein, to avoid cross-excitation between GFP and LD540 in the lipotoxicity assay. This vector was

transfected using polyethylenimine into HEK293T packaging cells at 80% confluence together with psPAX2 and pMD2G. Cell culture supernatant from the packaging cells was collected 48 and 72 h posttransfection, filtered through a 0.2 μm filter, and concentrated by ultracentrifugation at 50,000 g for 90 min. The viral pellet was resuspended in infection medium consisting of EM (10 μM Y-27632) and 8 $\mu\text{g}/\text{ml}$ polybrene and stored at -80°C .

Prior to transduction, healthy control and DGAT1-deficient organoids were grown in EM for 2–3 days. The organoids (2/24 wells) were then dissociated into single cells using TrypLE and resuspended in 250 μl infection medium in a 48-well suspension cell culture plate. Virus transduction was performed as reported previously (22). In brief, 10 μl of high-titer virus was added to the cell suspension and mixed by gentle pipetting. The plate was centrifuged at 450 g at 32°C for 1 h. The plate was then incubated at 37°C for an additional 6 h. The cells were spun down and resuspended in 2:1 Matrigel with EM, seeded into two wells of a 24-well tissue culture plate, and grown in EM + 10 μM Y-27632. Three days after transduction, the medium was changed to EM with 100 $\mu\text{g}/\text{ml}$ hygromycin B. When growth in hygromycin-resistant organoids was apparent, the organoids were split and cultured in EM.

Quantification and statistical analysis

Data are presented as mean \pm SD. Statistical significance was evaluated by paired two-way ANOVA within families with Tukey's post hoc (Fig. 1B, C) or Bonferroni's post hoc (Figs. 2B; 4D, H), unpaired two-tailed Student's t -test (Fig. 3E), unpaired two-way ANOVA across families with Tukey's post hoc (Fig. 5D), and paired two-way ANOVA for simple comparisons to the baseline within families with Dunnett's post hoc (Fig. 6C, D). For comparisons of LC_{50} values, the two-way ANOVA was carried out for 31 (Fig. 4D, H) or 19 (Fig. 5D) degrees of freedom. Concentration curves were fitted to a nonlinear regression with variable slope with a range constraint from 0% to 100%. Each organoid line was measured in duplicate (unless otherwise stated), of which the average was pooled per group (control or patient). All statistical analyses were performed using GraphPad Prism 7 software. Individual experiments, the exact value of n , and further details of analysis are stated in the corresponding Methods section. Significance was defined as $P < 0.05$, and visual representations of P -values are summarized in the figure legends.

RESULTS

DGAT2 mediates LD formation in absence of DGAT1

We have previously shown that although human intestinal stem cell-like organoids from patients with a loss-of-function mutation in *DGAT1* produced significantly less TG-containing LDs upon stimulation with OA compared with healthy controls (10), LD formation was not completely absent. Because TGs can also be produced by the functional isozyme, DGAT2, we considered DGAT2 to be the most likely candidate responsible for the residual LD formation in these DGAT1-deficient cells.

To determine whether DGAT2 function contributes to the formation of the remaining LDs, we incubated stem cell-like organoids for 16 h with OA in the absence or presence of either a specific D2i, a specific D1i, or both (D1i+D2i). We stained LDs by using the LD-specific dye, LD540, and performed confocal microscopy to

characterize the pattern of LD formation in whole organoids. As shown previously, we found that LD formation was partially inhibited [Fig. 1A and (10)] in the absence of functional DGAT1, as demonstrated by a less consistent radial staining pattern surrounding the nuclei. Surprisingly, we found that D2i treatment in DGAT1-deficient organoids completely abolished LD formation, whereas LD formation in control organoids was not affected by inhibition of DGAT2 (Fig. 1A). For statistical analyses, LD formation was quantified by flow cytometry by measuring mean fluorescent intensity (MFI) of LD540 (Fig. 1B) and mean side scatter area (SSC-A; an indicator for granularity), as the mean SSC-A of individual cells increases upon LD formation (Fig. 1C). As such, we show that double inhibition of DGAT1 and DGAT2 (D1i + D2i) in control organoids resulted in a complete lack of LD formation in intestinal stem cells (Fig. 1B, C). These data indicate that LD formation in response to OA is mediated mainly by DGAT1, and DGAT2 is able to partially rescue LD formation in the absence of functional DGAT1.

Because previous studies suggested that DGAT2 is expressed at very low levels in human intestine (15, 16), we quantified DGAT2 gene and protein expression in human intestinal biopsy-derived organoids from healthy controls and DGAT1-deficient patients. Western blotting revealed that DGAT1 protein was detected in control organoids and human ileum epithelium tissue, whereas DGAT2 protein was detected in both healthy and patient organoids as well as in ileum tissue (Fig. 2A). In addition, we show that levels of DGAT1 protein were increased, while DGAT2 protein expression was decreased when the organoids were driven toward an enterocyte phenotype by incubating organoids with DM (Fig. 2B). These data indicate that both DGAT1 and DGAT2 are expressed in human intestinal epithelium; however, mature enterocytes express higher levels of DGAT1 and lower levels of DGAT2, compared with stem cell-like epithelial cells.

DGAT1-deficient cells produce larger LDs compared with control cells

Previous studies have shown that DGAT2, but not DGAT1, can localize to existing LDs and incorporate additional TG into the growing droplet (12–14). These expanding LDs carry multiple enzymes of the TG synthesis machinery and, as a result, grow larger than LDs lacking this system (14). As a result, it has been shown that DGAT1-deficiency in mouse intestine leads to a decrease in LD number but an increase in LD size, and vice versa (23).

Therefore, we hypothesized that those LDs that were observed in DGAT1-deficient human intestinal organoids, would also be structurally different from LDs in healthy organoids. We quantified size and number of LDs upon stimulation with OA by electron microscopy (Fig. 3A–D) and observed significantly lower numbers of LDs in patient organoids compared with healthy controls (Fig. 3E). Furthermore, the surface area of individual LDs indicated that DGAT1-deficient organoids produced a specific population of LDs that were larger than $2.7 \mu\text{m}^2$ (13% of total LDs in DGAT1-deficient organoids vs. <1% in control organoids),

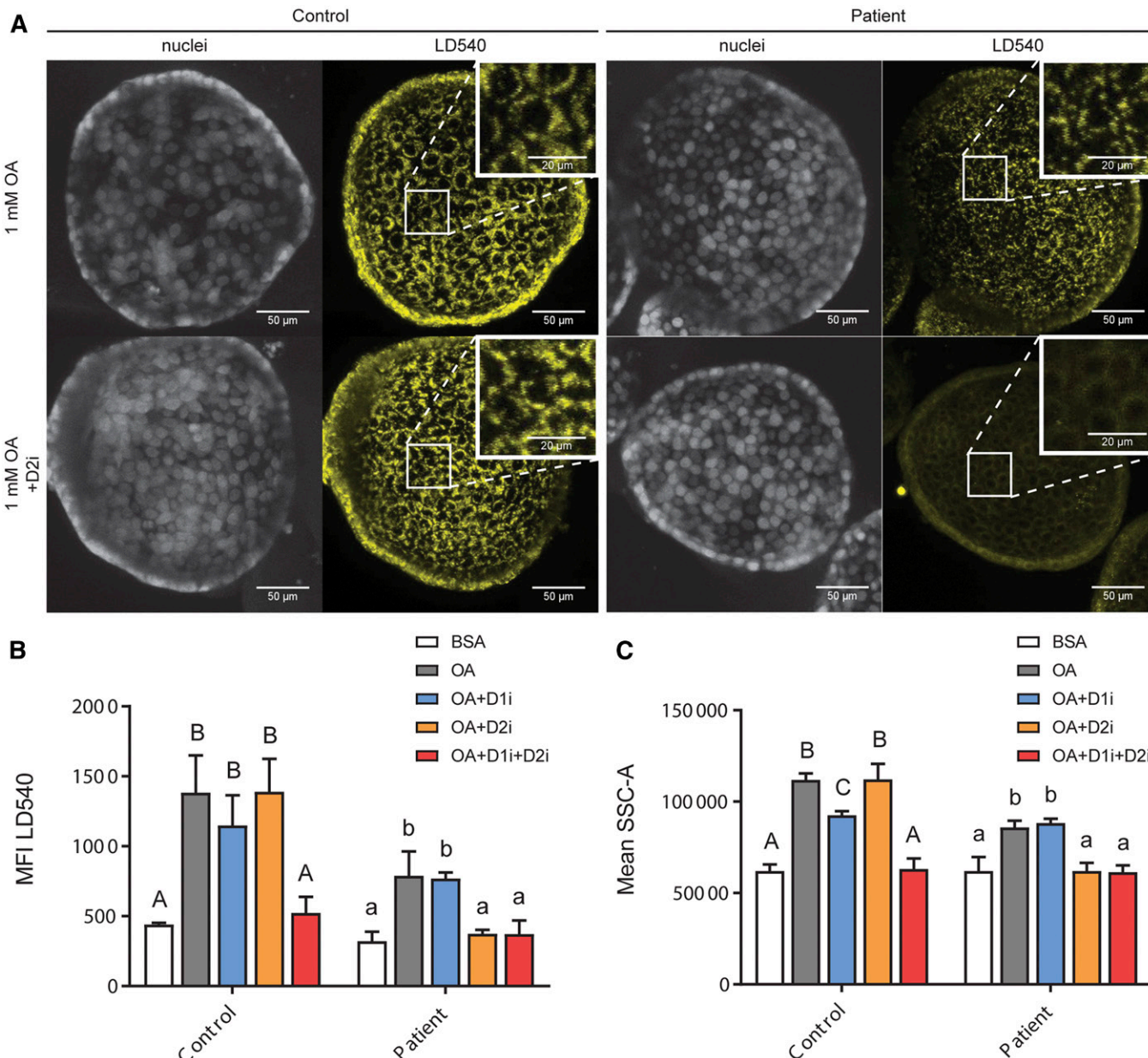


Fig. 1. DGAT2 is required for LD formation in the absence of DGAT1. Healthy control and DGAT1-deficient organoids were grown in EM and stimulated for 16 h with 1 mM OA, with or without D2i and stained for Hoechst (white) and LD540 (yellow). A: Representative fluorescent images at 20 \times magnification of three healthy controls and three patients; scale bars are 50 μ m. Inserts represent a higher magnification; scale bars are 20 μ m. B, C: Flow cytometry was used to determine MFI for LD540 (B) and mean SSC-A of organoids treated with BSA vehicle control [1 mM OA, OA + D1i, OA + D2i, or OA + D1i + D2i] (C). MFI and mean SSC-A were calculated for $n = 3$ per group and are representative of two independent experiments. Statistical analysis was done using a paired two-way ANOVA with controls and patients as separate families with a Tukey's multiple comparison test. Mean \pm SD is plotted; Bars with different letters are significantly different ($P < 0.05$).

in addition to the smaller LDs that were found in both types of organoids (Fig. 3F). These results show that DGAT1 and DGAT2 in human intestine work nonredundantly in epithelial lipid metabolism, as measured by the differences in LD formation. This is similar to the findings described for mouse ex vivo intestine (23).

DGAT2 protects against OA-induced toxicity in absence of DGAT1

DGAT1-mediated LD formation has been shown to protect against lipotoxicity in various contexts, such as lipid

stimulation or amino acid starvation in murine fibroblasts and adipocytes (7, 8, 24). We have previously shown that DGAT1-deficient human intestinal stem cell-like organoids were more sensitive to OA-induced lipotoxicity, but were resistant to low concentrations (2 mM) of OA (10). Because LD formation in DGAT1-deficient cells is dependent on DGAT2, we hypothesized that DGAT2-mediated LDs protect these stem cells from lipotoxicity as well. Therefore, we measured cell death by PI staining at a range of OA concentrations in the presence or absence of D1i and/or D2i. We have used the DNA stains, Hoechst (stains

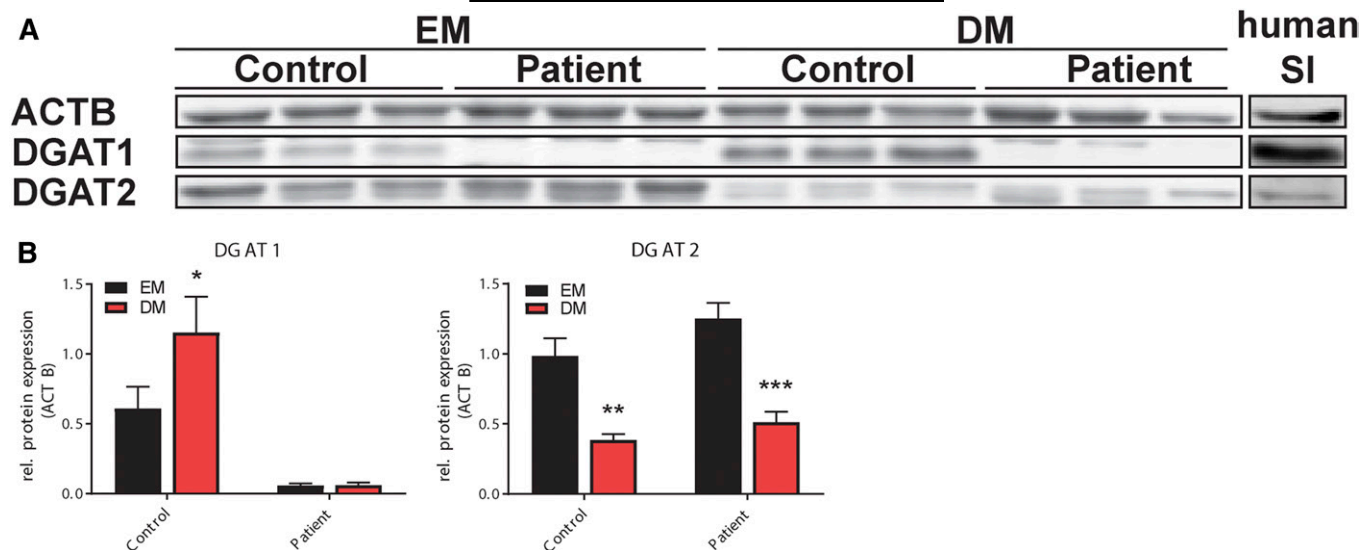


Fig. 2. DGAT1 and its isozyme, DGAT2, are expressed in human small intestine and human intestinal organoids. A: Western blot for DGAT1, DGAT2, and household protein actin (ACTB) on whole cell lysate from control ($n = 3$) and patient ($n = 3$) organoids grown on EM or DM and healthy control human ileum (SI) tissue ($n = 1$). B: Quantification of Western blot results, normalized to ACTB band intensity. Mean \pm SD is shown of three independent organoid lines. Statistical analysis was performed with a paired two-way ANOVA within families with Bonferroni multiple comparisons; * $P \leq 0.05$, ** $P \leq 0.01$, *** $P \leq 0.001$.

chromatin), as indicator for live organoids, and PI (only permeant for death cells), as indicator for dying organoids (Fig. 4A, supplemental Fig. S1A). To assess the concentration that is lethal to 50% of organoids (LC_{50}), we calculated the maximum assay response as a measure of the percentage of cell death by quantifying the area of PI and Hoechst staining for each condition and performing nonlinear regression analysis on the log-transformed concentration of OA (Fig. 4B, C; Table 1). We determined that control organoids were resistant to OA-induced lipotoxic stress up to an LC_{50} of 6.3 mM OA. As expected, control organoids that were treated with D1i and DGAT1-deficient patient-derived organoids were less tolerant to lipotoxic stress and show an LC_{50} of 3.3 mM and 2.8 mM OA, respectively. D2i treatment in control organoids did not increase the sensitivity to OA toxicity, although the combined treatment of both D1i and D2i significantly decreased the resistance to OA further than treatment with D1i alone ($LD_{50} = 2.6$ mM; Fig. 4B, D; Table 1). Likewise, D2i treatment in DGAT1-deficient organoids decreased their resistance to lipotoxic cell death to an LD_{50} of 2.4 mM (Fig. 4C, D; Table 1).

In summary, we here show that in absence of DGAT1, DGAT2 function partially rescues lipotoxic cell death of intestinal stem cells. Our data show that LDs produced by DGAT1 or DGAT2 have the potential to rescue intestinal epithelial cells from OA toxicity, indicating that the size of LDs does not influence their protective role in lipotoxicity.

Differentiated epithelial cells tolerate higher levels of OA

So far, our experiments were performed in stem cell-like organoids that were cultured in hSI-EM, also known as EM, which contains WNT3A and several inhibitors to maintain stemness and proliferation capacity (18). However, mature enterocytes located on the villus-domain of the gut

epithelium presumably suffer from much more exposure to FAs (25). Furthermore, DGAT1 deficiency was recently shown to impact mostly differentiated enterocytes (26). Therefore, we set out to determine the sensitivity to lipotoxicity in differentiated epithelial cells as well, and organoids were cultured for 5 days in EM and subsequently incubated in DM for 5 days, which induces differentiation toward an enterocyte phenotype. Surprisingly, we found that differentiated control organoids were not susceptible to lipotoxicity at concentrations up to 10 mM OA (Fig. 4E, F, H; supplemental Fig. S1B; Table 1). In concordance with the results in EM, lack of DGAT1 increased the sensitivity of differentiated DGAT1-deficient ($LC_{50} = 6.0$ mM; Fig. 4G, H; Table 1) or D1i-treated control ($LC_{50} = 5.3$ mM; Fig. 4F, H) organoids. However, in contrast to the stem cell-like organoids, there was no significant effect of additional D2i on lipotoxicity tolerance in either control or patient organoids. These findings indicate that differentiated enterocytes tolerate higher levels of OA compared with stem-cell like organoids. In concordance with the lower DGAT2 protein expression we found in differentiated enterocytes, DGAT2 has no apparent functional role in the differentiated epithelium, even in the absence of DGAT1.

OA-dependent resistance to PA toxicity is partially regulated by DGAT2

Our data indicate that DGAT2 is of little significance in healthy intestinal epithelium, although DGAT2 function could partially rescue LD formation and protect DGAT1-deficient cells from OA toxicity. However, lipids in the human diet consist of a mixture of UFAs and SFAs. The most common dietary SFA, PA, has been shown to be more toxic than OA in a variety of tissues, such as mouse fibroblasts, rat insulin-producing cells, and hepatocytes (24, 27–29). Therefore, we next determined the role of intestinal DGAT

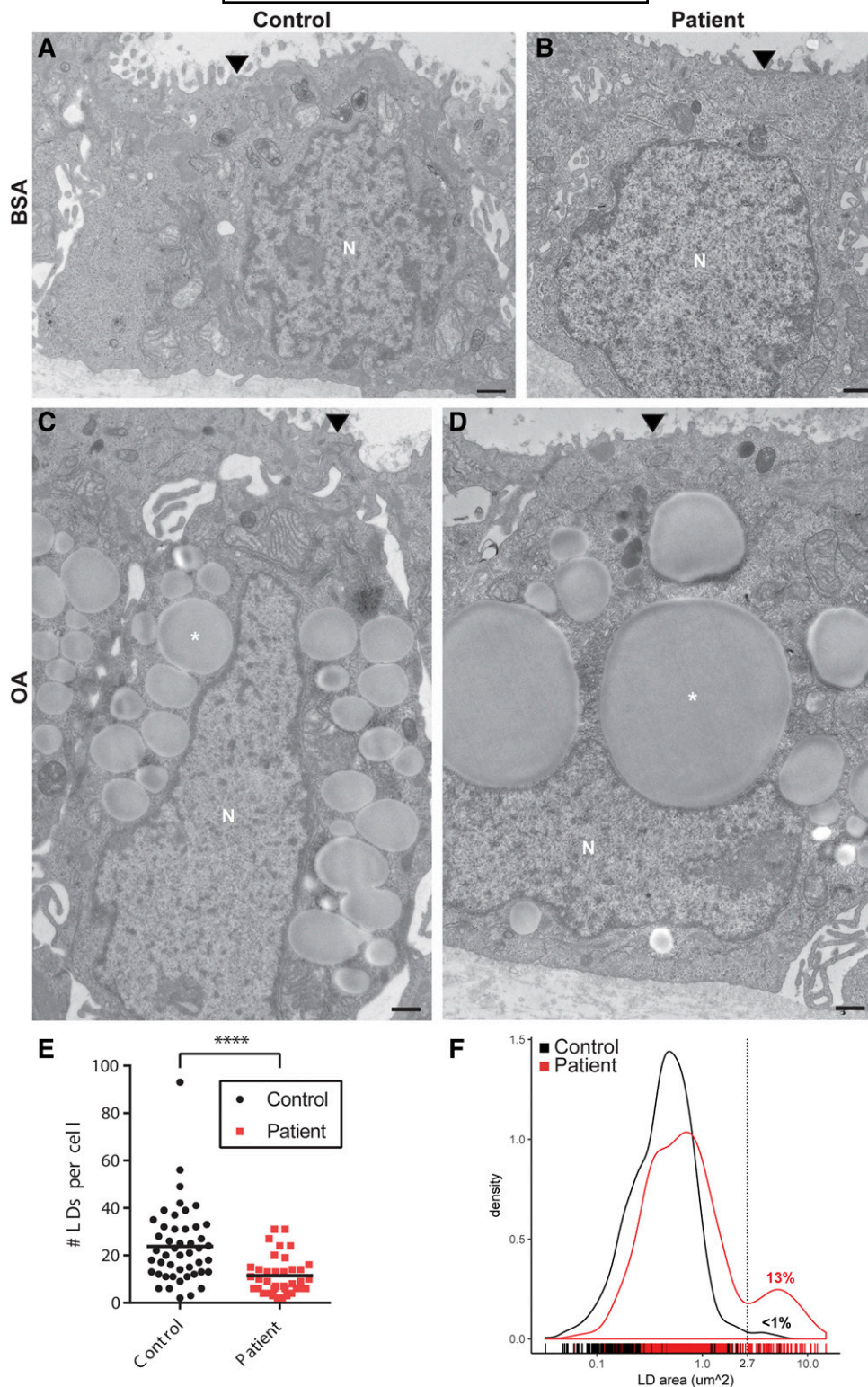


Fig. 3. DGAT1-deficient intestinal epithelial cells produce a lower number of LDs with an increased surface area upon incubation with OA. Representative transmission electron microscopy cross-section images of healthy control organoids grown in EM and stimulated for 16 h with BSA (A) or 1 mM OA (C) and DGAT1-deficient organoids stimulated for 16 h with BSA (B) or 1 mM OA (D). Apical membrane (arrowhead), nucleus (N) and LD (*, one indicated per image) are indicated. Scale bars are 1 μm . E, F: Quantification of LD number per cell (E) and density plot for the size of individual LDs per cell (F), counted for 20 cells per organoid line, three lines per group. E: Mean \pm SD is shown, statistical analysis performed with an unpaired *t*-test; **** $P \leq 0.0001$. F: Percentage of LDs > 2.7 μm^2 (dotted line) is indicated per group.

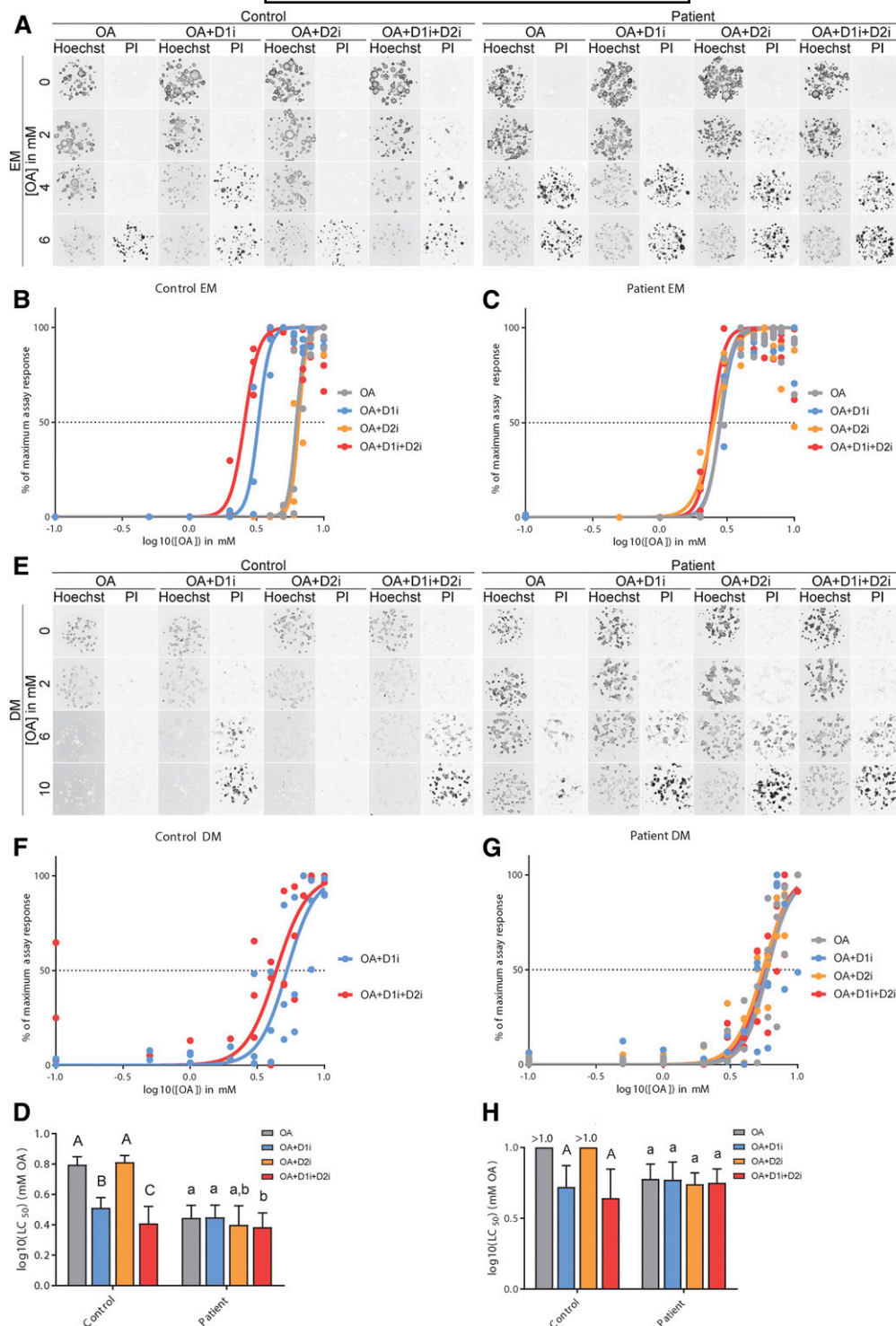


Fig. 4. DGAT2 is required for resistance to OA-induced toxicity in the absence of DGAT1. Control (left panel) and patient organoids (right panel) were cultured in EM (A–D) or DM (E–H) and stained for Hoechst and PI to measure cell death. The cells were stimulated for 16 h with OA, OA + D1i, OA + D2i, or OA+D1i+D2i. A, E: Representative fluorescent images for Hoechst and PI for each condition. Complete data set in supplemental Fig. S2. B, C, F, G: Quantification of the total area of PI fluorescence plotted against the log₁₀([OA]), fitted with nonlinear regression with variable slope to calculate LC₅₀ (dotted lines) of control samples (B, F) and patient samples (C, G). In F, lines for OA and OA + D2i were omitted due to lack of assay response. D, H: Mean LC₅₀ ± SD (n = 3) of the regression analysis for each condition. The area of PI fluorescence is the average of technical replicates for each donor, plotted as one data point in the regression analysis. The LC₅₀ was calculated from the combined three independent control or patient organoid lines. ND (not defined), no cell death was measured. Statistical analysis was performed using an unpaired two-way ANOVA on the average log₁₀(LC₅₀) ± log₁₀(SE) with controls and patients as separate families with Bonferroni's post hoc; bars with different letters are significantly different (P < 0.05).

TABLE 1. Quantification of organoid resistance to OA toxicity as represented in Fig. 4

Condition	EM		DM	
	Control	Patient	Control	Patient
OA	6.3 [6.0–6.5] ^A	2.8 [2.6–3.0] ^a	>10 ND	6.0 [5.5–6.5] ^a
OA + D1i	3.3 [3.1–3.4] ^B	2.8 [2.6–3.0] ^a	5.3 [4.6–6.0] ^A	5.9 [5.3–6.6] ^a
OA + D2i	6.5 [6.3–6.7] ^A	2.5 [2.3–2.8] ^{a,b}	>10 ND	5.5 [5.2–5.9] ^a
OA + D1i + D2i	2.6 [2.3–2.8] ^C	2.4 [2.2–2.6] ^b	4.4 [3.7–5.2] ^A	5.6 [5.2–6.1] ^a

Values are shown as the LC₅₀ values with 95% confidence interval in brackets, transformed from the log₁₀ regression results into a linear scale, resulting in OA concentrations (millimolar) where 50% of organoids are PI positive. Cells with different letters (i.e., A, a, etc.) within experiments in EM or DM are significantly different (*P* < 0.05). ND, LC₅₀ was not determined, and statistical interpretation was not possible.

enzymes in SFA metabolism and the contribution of DGAT2 therein. As our results indicate that DGAT2 is mostly expressed in the intestinal stem cell niche and DGAT2 inhibition only has an effect on patient cells cultured in EM, we performed this experiment in stem cell-like organoids. In addition, we studied the role of DGAT1 in the resistance to PA toxicity by using patient-derived organoids.

We incubated stem cell-like healthy and DGAT1-deficient organoids with various concentrations of PA for 16 h in the absence (Fig. 5A, supplemental Fig. S2A) or presence (Fig. 5B, supplemental Fig. S3B) of a nonlethal dose of OA (1 mM), and determined cell death by PI staining. We found that PA was indeed more toxic than OA for intestinal stem cells, because cell death of healthy control organoids occurred at an LC₅₀ of 1.1 mM PA (Fig. 5A, C, D; Table 2), whereas OA toxicity showed an LC₅₀ of 6.3 mM (Fig. 4A). In line with earlier studies (24), DGAT1 deficiency did not significantly influence the toxicity of PA, leading to a LC₅₀ of 1.2 mM in DGAT1-deficient organoids (Fig. 5C, D). However, in contrast to an earlier report in rat hepatocytes (28), D2i in DGAT1-deficient human intestinal organoids slightly, but significantly, decreased the resistance to PA (Fig. 5C, D; Table 2), while D2i in control organoids did not. These data indicate that DGAT2 also has a functional role in PA tolerance of human intestinal stem cells, but only in the absence of DGAT1.

It was previously shown that OA-induced LDs were required to protect mammalian cells from PA toxicity (24). Because DGAT2 is able to expand existing LDs, we hypothesized that DGAT2 plays a significant role in the OA-mediated resistance to PA toxicity by incorporating PA in existing OA-containing LDs. Here, we show that combined stimulation of PA and 1 mM OA increased the lipotoxicity resistance of both control (LC₅₀ = 2.4 mM) and patient-derived stem cell-like organoids (LC₅₀ = 2.0 mM) (Fig. 5B, C, D), in a partially DGAT1-dependent manner (Fig. 5C, D). Moreover, this rescuing effect of OA was also partially dependent on DGAT2 in patient organoids (LC₅₀ = 1.8 mM) but not in control organoids (LC₅₀ = 2.3 mM). OA-dependent rescue of PA lipotoxicity was however not completely dependent on function of DGAT1 and DGAT2, as indicated by the lower tolerance to PA of patient organoids treated with D2i (LC₅₀ = 1.1 mM PA) versus D2i treatment in the presence of OA (LC₅₀ = 1.8 mM PA). These data indicate that OA has an additional protective role in PA toxicity independent of DGAT enzymes, which is not yet understood.

Finally, we show that PA stimulation alone barely resulted in LD formation, while PA+OA stimulation greatly increased the number of LDs (Fig. 5E), indicating that the PA lipotoxicity dynamics correlated with OA-dependent LD formation. In summary, we conclude that OA-induced resistance to PA in intestinal stem cells is partially dependent on DGAT1, whereas in the absence of DGAT1, resistance to PA is partially dependent on DGAT2, both in the presence and the absence of OA.

OA- and PA-induced lipotoxicity is mediated by ER stress

In a previous study, we have shown that OA-induced toxicity leads to caspase-mediated cell death in intestinal organoids in a DGAT1-dependent manner (10). Our current data show that in absence of DGAT1, D2i sensitizes DGAT1-deficient intestinal stem cells to FA-induced lipotoxicity. However, the mechanism of caspase activation during FA-mediated cell death in human intestinal cells is not yet fully understood.

Recently, it has been shown that DGAT1 expression was required to protect adipocytes from FA-induced ER stress during lipolysis (8). Therefore, we hypothesized that high levels of FA in intestinal epithelium trigger apoptotic cell death by inducing ER stress. ER stress is a state of disequilibrium in the ER and can be caused by a variety of factors, including toxicants, an overload of unfolded proteins, or perturbation of the ER lipid bilayer (30–32). These various stressors activate the unfolded protein response (UPR) signaling pathway, which is dependent on the receptors, inositol requiring enzyme 1 (IRE1), double-stranded RNA-activated protein kinase-like ER kinase (PERK), and activating transcription factor 6 (ATF6) (Fig. 6A).

We measured activation of the UPR pathways by analyzing the expression of (un)spliced XBP1, transcription factor C/EBP homologous protein (CHOP), and BiP (chaperone from the heat shock protein HSP70 family), which are targets downstream of IRE1, PERK, and ATF6 signaling, respectively (33). Because UPR signaling precedes cell death, and we have shown extensive cell death upon 16 h of FA stimulation, we stimulated organoids for 10 h with various amounts of OA (Fig. 6B) or PA (Fig. 6C).

We performed RT-qPCRs to determine RNA expression of total XBP1 (tXBP1) and spliced XBP1 (sXBP1), CHOP, and BiP and found that the amount of sXBP1 versus tXBP1,

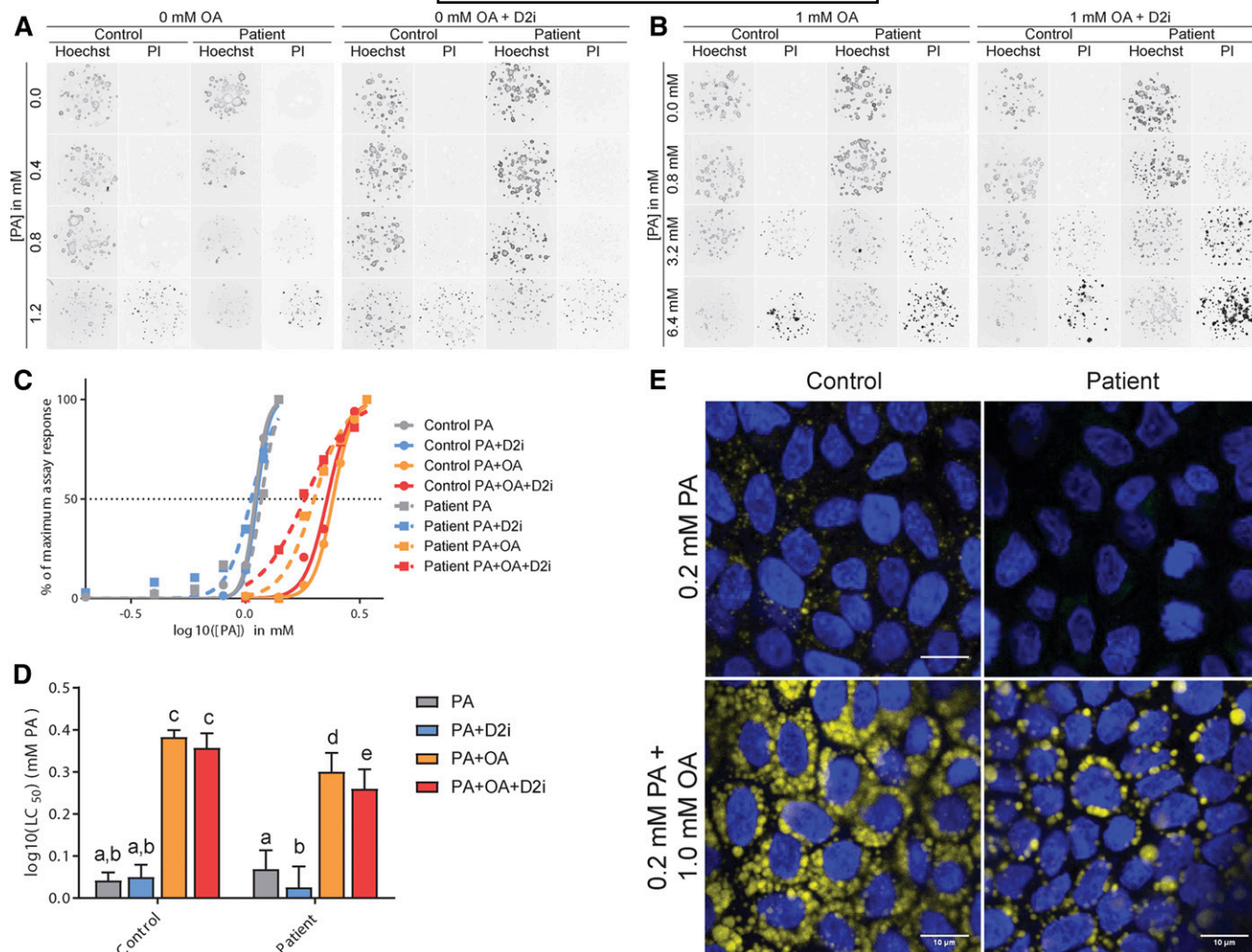


Fig. 5. OA-dependent rescue of PA lipotoxicity is dependent on DGAT1-mediated LD formation. Control and patient organoids were grown in EM and stimulated for 16 h with a concentration series of PA in the absence or presence of D2i, with or without the addition of a nonlethal dose of OA (1 mM) and stained for Hoechst and PI to measure cell death. A, B: Representative fluorescent images for Hoechst and PI staining for each condition. Complete data set is in supplemental Fig. S3. C: Quantification of the total area of PI fluorescence plotted against the $log_{10}([PA])$, fitted with nonlinear regression with variable slope to calculate LC_{50} (dotted line) for each condition as described for Fig. 4. D: Mean $LC_{50} \pm SD$ (n = 3) of the regression analysis for each condition. Statistical analysis was performed using a two-way ANOVA on the average $log_{10}(LC_{50}) \pm log_{10}(SE)$ with Tukey's post hoc. Bars with different letters are significantly different ($P < 0.05$). E: Representative images of Hoechst (blue) and LD540 (yellow) staining to visualize LD formation in control and patient organoids stimulated with PA (top) or PA + 1 mM OA (bottom).

CHOP, and BiP were all upregulated upon incubation with 4 and 6 mM OA in healthy control organoids and already detectable upon incubation with 2 mM OA in DGAT1-deficient

TABLE 2. Quantification of organoid resistance to PA toxicity as represented in Fig. 5

Condition	EM	
	Control	Patient
PA	1.10 [1.08–1.12] ^{a,b}	1.17 [1.12–1.23] ^a
PA + D2i	1.12 [1.09–1.16] ^{a,b}	1.06 [1.01–1.12] ^b
PA + OA	2.41 [2.37–2.46] ^c	2.00 [1.91–2.10] ^d
PA + OA + D2i	2.28 [2.19–2.37] ^c	1.82 [1.73–1.91] ^c

Values are shown as the LC_{50} values with 95% confidence interval in brackets, transformed from the log_{10} regression results into a linear scale, resulting in PA concentrations (mM) where 50% of organoids are PI positive. Cells with different letters (i.e., a, b, etc.) are significantly different ($P < 0.05$).

patient organoids (Fig. 6B). These results indicate increased ER stress levels in DGAT1-deficient organoids upon stimulation with increasing concentrations of OA, which finally results in apoptosis.

To determine whether UPR signaling is involved in PA toxicity as well, we performed real time-qPCR upon PA stimulation and found that the ratio of s/tXBP1 was strongly increased at 0.6 mM PA and higher concentrations in both control and patient organoids (Fig. 6C). In addition, both CHOP and BiP were upregulated at PA concentrations of 1.0 mM and higher in both control and patient organoids. These results indicate that PA induces ER stress at lower concentrations compared with OA. In concordance with our data of PA lipotoxicity, we did not observe an effect of DGAT1 deficiency under these conditions.

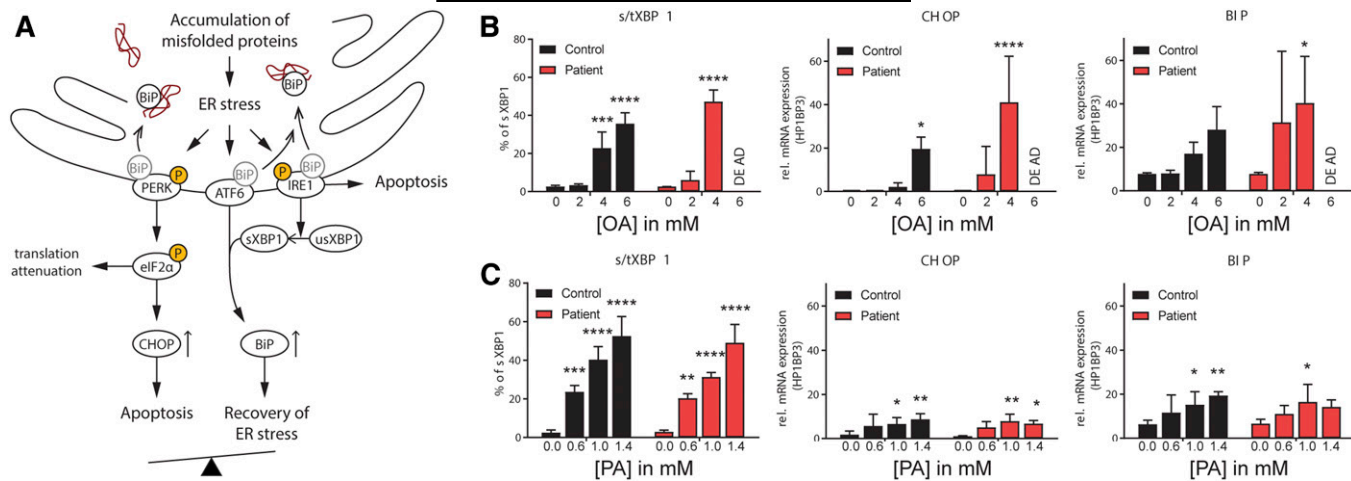


Fig. 6. High concentrations of FAs induce ER stress. A: A schematic overview of canonical UPR signaling, adapted from (33, 50). B, C: Control and patient-derived organoids grown on EM were incubated for 10 h with a concentration range of OA (B) or PA (C), and RT-qPCR was performed for downstream UPR signaling targets. Data points are the average of technical duplicates for control (n = 3) and patient (n = 3) organoid lines. Statistical analysis was performed by paired two-way ANOVA for simple comparisons to the baseline within families with Dunnett's post hoc; * $P \leq 0.05$, ** $P \leq 0.01$, *** $P \leq 0.001$, **** $P \leq 0.0001$.

These data show that activation of the UPR pathways preceded OA- or PA-induced cell death, and therefore we conclude that FA-induced lipotoxicity in intestinal stem cells is mediated by induction of ER stress.

Overexpression of DGAT2 reduces sensitivity to lipotoxic stress

Previously, we have shown that overexpression of DGAT2 in DGAT1-deficient fibroblasts significantly restored the production of LDs upon OA stimulation (10). Therefore, we hypothesized that overexpression of DGAT2 in patient-derived intestinal organoids could reduce the sensitivity to lipotoxicity as well and could rescue the patients' phenotype. To investigate this, we transduced both control and patient organoids with a lentiviral overexpression construct of DGAT2 or GFP as control (supplemental Fig. S3A, B) and confirmed DGAT2 overexpression by Western blot (supplemental Fig. S3C, D). Next, we incubated transduced DGAT2 overexpressing (D2OE) and vector control (GFP) organoids with various concentrations of OA for 16 h, determined cell death by PI staining (supplemental Fig. S4), and calculated the LC_{50} in both stem cell-like (EM) and differentiated (DM) conditions (Fig. 7). In concordance with our finding that control organoids do not depend on DGAT2 function, DGAT2 overexpression or D2i treatment alone did not affect the sensitivity to OA lipotoxicity in control stem cell-like or differentiated organoids (Fig. 7B, D). However, DGAT2 overexpression completely restored the OA resistance of DGAT1-deficient patient organoids as well as D1i-treated control organoids in both EM and DM, which was fully inhibited by D2i treatment (Fig. 7B, D). These data show that increased expression of DGAT2 fully prevents lipid-induced toxicity of DGAT1-deficient intestinal organoids in both a stem cell-like and enterocyte-like state, indicating that induction of DGAT2 could serve as a novel therapeutic intervention in the treatment of DGAT1-deficient patients.

DISCUSSION

It has been shown that DGAT1-dependent LD formation protects against FFA toxicity in a variety of murine tissues (7, 8, 28). Recently, we have described a similar role for DGAT1 in human intestinal epithelium, as DGAT1-deficiency resulted in reduced LD formation and increased sensitivity to lipotoxicity of epithelial cells in vitro (10). These findings correspond with human clinical trials studying DGAT1 inhibition, which caused severe diarrhea in a dose-dependent manner (34, 35), similar to the diarrhea, vomiting, and intestinal failure that has been described as a result of DGAT1 deficiency (10, 15, 26, 36, 37). Based on these data, we proposed that DGAT1 is required in the intestine to protect the epithelial cells from the toxicity of dietary lipids. In the absence of DGAT1, the epithelium lacks this protection, which causes cell death and results in PLE (10). However, the mechanism by which DGAT1 protects the intestine from lipotoxicity and the key-players in this process have not yet been reported. Here, we show that both DGAT1 and DGAT2 mediate lipid metabolism in intestinal stem cells, which protect these cells from FA-induced cell death.

Specifically, our data indicate that DGAT1 is important to prevent intestinal epithelial ER stress in both stem cells and enterocytes during high fat conditions. These findings are consistent with earlier reports indicating an important role for DGAT1 in cellular lipotoxicity. For instance, several transgenic mouse models of tissue-specific DGAT1 overexpression have reported a beneficiary role for DGAT1 in ER protection (38–40), and a heart-specific deletion of DGAT1 increased lipotoxicity of cardiomyocytes (40). Furthermore, it has been shown that DGAT1 and DGAT2 activities could compensate for each other to produce TG in murine adipocytes, whereas in lipolytic conditions, only DGAT1 activity prevented ER stress-induced cell death (8).

The role of DGAT2 in the human intestinal epithelium has not been the subject of extensive study to date because

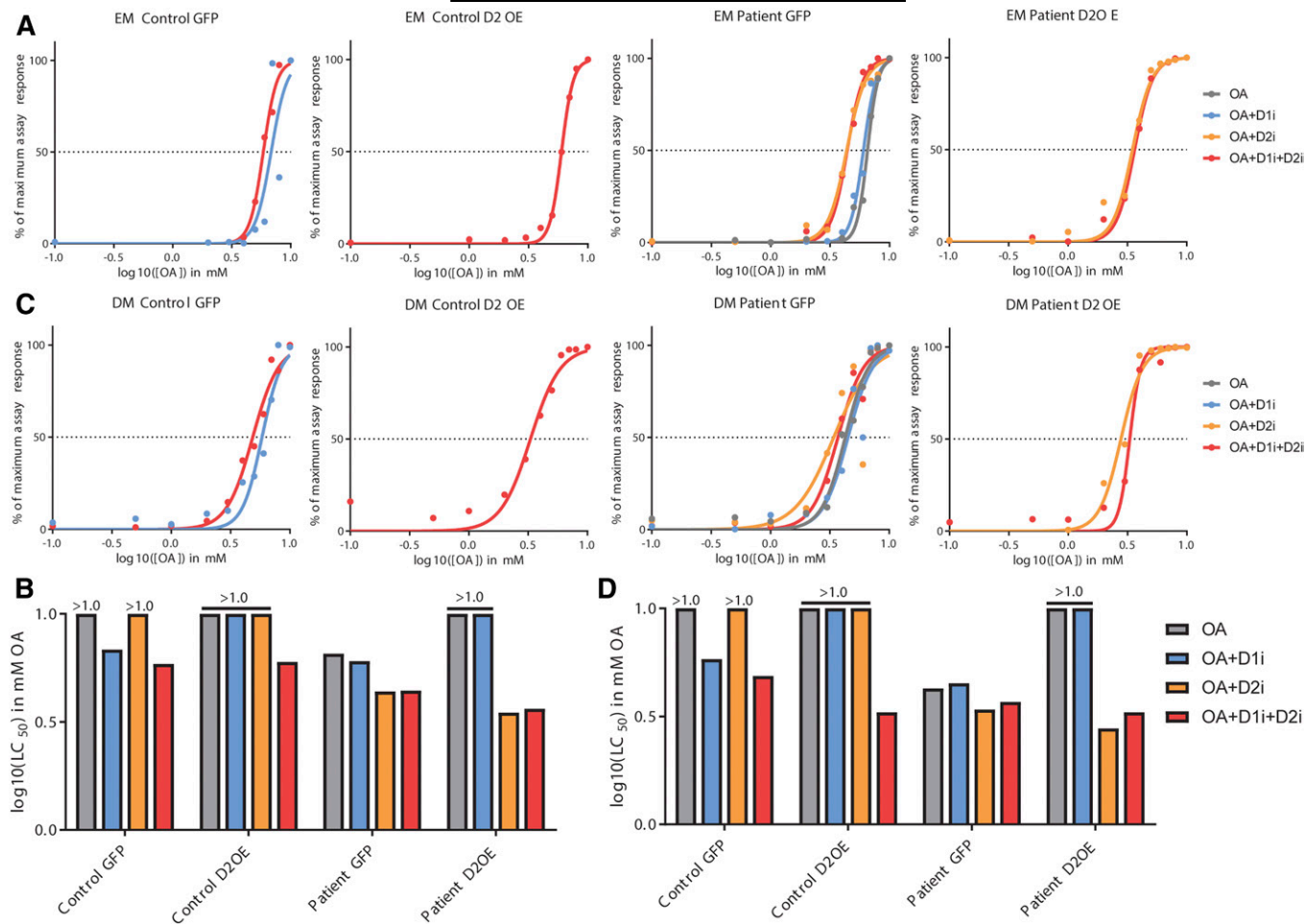


Fig. 7. Overexpression of DGAT2 in DGAT1-deficient organoids rescues increased sensitivity to lipotoxicity. Control ($n = 1$) and patient ($n = 1$) organoid lines were transduced with a lentiviral vector to accommodate DGAT2 overexpression (D2OE). Nontransduced or D2OE organoids were grown in EM (A, B) or DM (C, D) and incubated for 16 h with a concentration range of OA in the presence of D1i (OA + D1i), D2i (OA + D2i), or both (OA + D1i + D2i). Organoids were stained for Hoechst and PI to measure cell death (supplemental Fig. S3) and quantification of the total area of PI fluorescence plotted against the log₁₀([OA]) was fitted to a nonlinear regression with variable slope to calculate LC₅₀ (dotted line) (A, C) as described for Fig. 4. B, D: LC₅₀ values (single measurement) of the regression analysis for each condition.

DGAT2 expression was detected only at very low levels and therefore believed to have no functional role (15, 16). However, mouse studies have shown that DGAT2 in the intestinal epithelium had an effect on LD formation in number and size (23, 28, 41, 42). In this study, we show for the first time that the human intestine expresses functional DGAT2 in the epithelial stem cell niche, although its role is only evident in the absence of functional DGAT1. This is in concordance with the findings that a patient with a *DGAT2* missense mutation (p.Y223H) did not demonstrate an intestinal phenotype (43). Furthermore, it has been shown that *Dgat1*^{KO} mice, which do express *Dgat2* in mature enterocytes, do not exhibit an intestinal phenotype (44). In contrast, we have shown here that DGAT1-deficient patients who express DGAT2 in their intestinal crypts but not in differentiated cells, still suffer from intestinal symptoms. This indicates that DGAT2 can only sufficiently compensate for the role of DGAT1 when its expression is induced in mature enterocytes.

Furthermore, we characterized DGAT2-dependent LD formation in DGAT1-deficient intestinal stem cells and

found a population of large LDs in addition to the smaller LDs formed in presence of DGAT1. The finding that only some, but not all, LDs grow larger in the absence of DGAT1 corresponds with a study performed on *Drosophila* S2 cells and mouse embryonic fibroblasts (14). This study has shown that the TG synthesis machinery, including DGAT2, is recruited to the surface of some LDs and is required to generate larger LDs after initial formation. However, it is currently unknown if these larger LDs fulfill an alternate function compared with the smaller LDs, or if this localization of DGAT2 to the LD surface occurs in human tissue as well.

As reported previously, CMs are held within secretory vesicles (23, 45, 46) inside the absorptive enterocyte. Although we did not observe such secretory lipid vesicles in the organoid cells on the electron microscope images, we cannot exclude the possibility that the lower number of LDs observed in DGAT1-deficient organoids might be an effect of more CM synthesis at an earlier time point. Therefore, further research should be performed to elucidate the potential role of CM synthesis in DGAT1-deficient patients.

In addition, further research should be performed to determine whether the fate of FAs, such as LD and/or CM formation, is different when FAs are taken up at the basolateral side (as in our 3D organoid model) or at the apical side (as in dietary uptake).

In the stem cell-like organoids, our data clearly indicate a functional role for DGAT2 in the absence of DGAT1. However, we could not determine a functional role for DGAT2 in differentiated epithelial cells. We have found that intestinal stem cells, but not differentiated enterocytes, express DGAT2 in human intestinal organoids. Since DGAT1 is of most vital importance in our model system, and DGAT2 deficiency did not result in a clear intestinal phenotype (43), it is not yet clear why intestinal stem cells express functional DGAT2 and downregulate it upon differentiation.

How DGAT2 function is lost during differentiation of human intestinal epithelial cells, whereas murine mature enterocytes do express *Dgat2* (44), is currently unknown. A likely explanation is provided by our observation that DGAT2 mRNA and protein are downregulated in differentiated cells compared with stem cell-like cells. Otherwise, DGAT2 protein activity or stability could be subject to post-translational regulation through phosphorylation, as multiple protein kinase C target sites have been identified in the DGAT2 amino acid sequence (47).

The loss of DGAT2 during differentiation of enterocytes is especially interesting in light of a recent study on the effects of a long-term HFD on the risk of colorectal cancer in mice. This study shows that HFD-induced obesity elicits changes in the DNA methylome of the intestine, which affects gene expression patterns in the epithelium (3). Interestingly, the epithelial response of HFD-fed mice included a significant upregulation of DGAT2, but not DGAT1, indicating that DGAT2 is important for protection of the intestinal epithelium against high fat loads.

Our data suggest that DGAT1 is required for LD-mediated resistance to lipid-induced ER stress in the intestinal epithelium, although it is currently unknown how LD formation relieves stress from the ER. Because excess FA in the ER membrane has been shown to trigger the UPR by directly inducing IRE1 α and PERK phosphorylation (30), less efficient storage of FAs is likely to be the direct cause of ER stress. If the extracellular FA concentrations do not subside, and excess FAs cannot be stored in LDs, the resulting ER stress will become severe enough to reach the threshold for induction of apoptosis. Our data show that OA- and PA-induced lipotoxicity are associated with markers of ER stress; however, rescue experiments will be required to determine causal relationships.

As was shown in earlier research, increased ER stress is also linked to mislocalization of apical transporters in the intestinal epithelium (48) and can thereby induce a primary epithelial malfunction resulting in diarrhea. Recently, mislocalization of apical transporters and cell-junction proteins was also reported in DGAT1-deficient Caco-2 cells, when lipids were added to the culture medium (26). It is currently unknown whether dietary lipids in DGAT1-deficient patients cause diarrhea either by lipotoxic

cell death and a resulting barrier breach or by defective intracellular trafficking and depolarization of enterocytes or both.

Although most DGAT1-deficient patients fare well with a lipid-restricted diet and intravenous administration of essential FAs (10, 26, 37), this therapeutic approach has a significant impact on the patients' quality of life. Here, we show that DGAT2 overexpression in intestinal organoids is able to rescue DGAT1-dependent sensitivity to lipotoxicity, indicating that DGAT2 might prove to be an alternative target for clinical therapy for DGAT1-deficient patients. Interestingly, it has been reported that long-term low-dose stimulation with PA favored a more stem cell-like phenotype in mouse intestinal organoids (49) and induced the upregulation of *Dgat2* mRNA expression through activation of Ppar δ signaling (3). Therefore, PPAR δ activation could provide a first target for the therapeutic upregulation of DGAT2 in the human intestinal epithelium.

The authors thank M. C. Hagemeijer, E. de Poel, and S. Suen for technical support with the confocal imaging; R. M. C. Scriwanek for assistance with transmission electron microscopy image presentation; T. Sommer for assistance with data acquisition; and B. Spee for generously providing LD540.

REFERENCES

- Kopelman, P. G. 2000. Obesity as a medical problem. *Nature*. **404**: 635–643.
- Renahan, A. G., M. Tyson, M. Egger, R. F. Heller, and M. Zwahlen. 2008. Body-mass index and incidence of cancer: a systematic review and meta-analysis of prospective observational studies. *Lancet*. **371**: 569–578.
- Li, R., S. A. Grimm, D. Mav, H. Gu, D. Djukovic, R. Shah, B. A. Merrick, D. Raftery, and P. A. Wade. 2018. Transcriptome and DNA methylome analysis in a mouse model of diet-induced obesity predicts increased risk of colorectal cancer. *Cell Rep*. **22**: 624–637.
- Yen, C. L., D. W. Nelson, and M. I. Yen. 2015. Intestinal triacylglycerol synthesis in fat absorption and systemic energy metabolism. *J. Lipid Res*. **56**: 489–501.
- Chavez-Jauregui, R. N., R. D. Mattes, and E. J. Parks. 2010. Dynamics of fat absorption and effect of sham feeding on postprandial lipemia. *Gastroenterology*. **139**: 1538–1548.
- Welte, M. A., and A. P. Gould. Lipid droplet functions beyond energy storage. *Biochim. Biophys. Acta Mol. Cell Biol Lipids*. **1862**: 1260–1272.
- Nguyen, T. B., S. M. Louie, J. R. Daniele, Q. Tran, A. Dillin, R. Zoncu, D. K. Nomura, and J. A. Olzmann. DGAT1-dependent lipid droplet biogenesis protects mitochondrial function during starvation-induced autophagy. *Dev. Cell*. **42**: 9–21.e5.
- Chitraju, C., N. Mejhert, J. T. Haas, L. G. Diaz-Ramirez, C. A. Grueter, J. E. Imbriglio, S. Pinto, S. K. Koliwad, T. C. Walther, and R. V. Farese, Jr. 2017. Triglyceride synthesis by DGAT1 protects adipocytes from lipid-induced ER stress during lipolysis. *Cell Metab*. **26**: 407–418.e3.
- Olzmann, J. A., and P. Carvalho. 2019. Dynamics and functions of lipid droplets. *Nat. Rev. Mol. Cell Biol*. **20**: 137–155.
- van Rijn, J. M., R. C. Ardy, Z. Kuloğlu, B. Härter, D. Y. van Haaften-Visser, H. P. J. van der Doef, M. van Hoesel, A. Kansu, A. H. M. van Vugt, M. Thian, et al. 2018. Intestinal failure and aberrant lipid metabolism in patients with DGAT1 deficiency. *Gastroenterology*. **155**: 130–143.e15.
- Braamskamp, M. J. A. M., K. M. Dolman, and M. M. Tabbers. 2010. Clinical practice: protein-losing enteropathy in children. *Eur. J. Pediatr*. **169**: 1179–1185.
- Kuerschner, L., C. Moessinger, and C. Thiele. 2008. Imaging of lipid biosynthesis: how a neutral lipid enters lipid droplets. *Traffic*. **9**: 338–352.

13. Stone, S. J., M. C. Levin, P. Zhou, J. Han, T. C. Walther, and R. V. Farese. 2009. The endoplasmic reticulum enzyme DGAT2 is found in mitochondria-associated membranes and has a mitochondrial targeting signal that promotes its association with mitochondria. *J. Biol. Chem.* **284**: 5352–5361.
14. Wilfling, F., H. Wang, J. T. Haas, N. Krahmer, T. J. Gould, A. Uchida, J. X. Cheng, M. Graham, R. Christiano, F. Fröhlich, et al. 2013. Triacylglycerol synthesis enzymes mediate lipid droplet growth by relocating from the ER to lipid droplets. *Dev. Cell.* **24**: 384–399.
15. Haas, J. T., H. S. Winter, E. Lim, A. Kirby, B. Blumenstiel, M. DeFelice, S. Gabriel, C. Jalas, D. Branski, C. A. Grueter, et al. 2012. DGAT1 mutation is linked to a congenital diarrheal disorder. *J. Clin. Invest.* **122**: 4680–4684.
16. Cases, S., S. J. Stone, P. Zhou, E. Yen, B. Tow, K. D. Lardizabal, T. Voelker, and R. V. Farese, Jr. 2001. Cloning of DGAT2, a second mammalian diacylglycerol acyltransferase, and related family members. *J. Biol. Chem.* **276**: 38870–38876.
17. Wiegand, C. L., A. R. Janicke, K. Schneeberger, G. F. Vogel, D. Y. van Haaften-Visser, J. C. Escher, R. Adam, C. E. Thöni, K. Pfaller, A. J. Jordan, et al. 2014. Loss of syntaxin 3 causes variant microvillus inclusion disease. *Gastroenterology*. **147**: 65–68.e10.
18. Sato, T., D. E. Stange, M. Ferrante, R. G. J. Vries, J. H. Van Es, S. Van den Brink, W. J. Van Houdt, A. Pronk, J. Van Gorp, P. D. Siersema, et al. 2011. Long-term expansion of epithelial organoids from human colon, adenoma, adenocarcinoma, and Barrett's epithelium. *Gastroenterology*. **141**: 1762–1772.
19. Rueden, C. T., J. Schindelin, M. C. Hiner, B. E. DeZonia, A. E. Walter, E. T. Arena, and K. W. Eliceiri. 2017. ImageJ2: ImageJ for the next generation of scientific image data. *BMC Bioinformatics*. **18**: 529.
20. Schindelin, J., I. Arganda-Carreras, E. Frise, V. Kaynig, M. Longair, T. Pietzsch, S. Preibisch, C. Rueden, S. Saalfeld, B. Schmid, et al. 2012. Fiji: an open-source platform for biological-image analysis. *Nat. Methods*. **9**: 676–682.
21. Campeau, E., V. E. Ruhl, F. Rodier, C. L. Smith, B. L. Rahmberg, J. O. Fuss, J. Campisi, P. Yaswen, P. K. Cooper, and P. D. Kaufman. 2009. A versatile viral system for expression and depletion of proteins in mammalian cells. *PLoS One*. **4**: e6529.
22. Koo, B. K., D. E. Stange, T. Sato, W. Karthaus, H. F. Farin, M. Huch, J. H. van Es, and H. Clevers. Controlled gene expression in primary Lgr5 organoid cultures. *Nat. Methods*. **9**: 81–83.
23. Hung, Y. H., A. L. Carreiro, and K. K. Buhman. Dgat1 and Dgat2 regulate enterocyte triacylglycerol distribution and alter proteins associated with cytoplasmic lipid droplets in response to dietary fat. *Biochim. Biophys. Acta Mol. Cell Biol. Lipids*. **1862**: 600–614.
24. Listenberger, L. L., X. Han, S. E. Lewis, S. Cases, R. V. Farese, D. S. Ory, and J. E. Schaffer. 2003. Triglyceride accumulation protects against fatty acid-induced lipotoxicity. *Proc. Natl. Acad. Sci. USA*. **100**: 3077–3082.
25. Hussain, M. M. 2014. Intestinal lipid absorption and lipoprotein formation. *Curr. Opin. Lipidol.* **25**: 200–206.
26. Schlegel, C., L. A. Lapierre, V. G. Weis, J. A. Williams, I. Kaji, C. Pinzon-Guzman, N. Prasad, B. Boone, A. Jones, H. Correa, et al. 2018. Reversible deficits in apical transporter trafficking associated with deficiency in diacylglycerol acyltransferase. *Traffic*. **19**: 879–892.
27. Gehrman, W., W. Würdemann, T. Plötz, A. Jörns, S. Lenzen, and M. Elsner. 2015. Antagonism between saturated and unsaturated fatty acids in ROS mediated lipotoxicity in rat insulin-producing cells. *Cell. Physiol. Biochem*. **36**: 852–865.
28. Leamy, A. K., C. M. Hasenour, R. A. Egnatchik, I. A. Trenary, C. H. Yao, G. J. Patti, M. Shiota, and J. D. Young. Knockdown of triglyceride synthesis does not enhance palmitate lipotoxicity or prevent oleate-mediated rescue in rat hepatocytes. *Biochim. Biophys. Acta Mol. Cell Biol. Lipids*. **1861** (9 Pt A): 1005–1014.
29. Plötz, T., B. Krümmel, A. Laporte, A. Pingitore, S. Persaud, A. Jörns, M. Elsner, I. Mehmeti, and S. Lenzen. 2017. The monounsaturated fatty acid oleate is the major physiological toxic free fatty acid for human beta cells. *Nutr. Diabetes*. **7**: 305.
30. Volmer, R., K. van der Ploeg, and D. Ron. 2013. Membrane lipid saturation activates endoplasmic reticulum unfolded protein response transducers through their transmembrane domains. *Proc. Natl. Acad. Sci. USA*. **110**: 4628–4633.
31. Rao, R. V., E. Hermel, S. Castro-Obrigon, G. del Rio, L. M. Ellerby, H. M. Ellerby, and D. E. Bredesen. 2001. Coupling endoplasmic reticulum stress to the cell death program. Mechanism of caspase activation. *J. Biol. Chem.* **276**: 33869–33874.
32. Kaufman, R. J. 1999. Stress signaling from the lumen of the endoplasmic reticulum: coordination of gene transcriptional and translational controls. *Genes Dev.* **13**: 1211–1233.
33. Osowski, C. M., and F. Urano. 2011. Measuring ER stress and the unfolded protein response using mammalian tissue culture system. *Methods Enzymol.* **490**: 71–92.
34. Denison, H., C. Nilsson, L. Löfgren, A. Himmelmann, G. Mårtensson, M. Knutsson, A. Al-Shurbaji, H. Tornqvist, and J. W. Eriksson. 2014. Diacylglycerol acyltransferase 1 inhibition with AZD7687 alters lipid handling and hormone secretion in the gut with intolerable side effects: a randomized clinical trial. *Diabetes Obes. Metab.* **16**: 334–343.
35. Meyers, C. D., K. Tremblay, A. Amer, J. Chen, L. Jiang, and D. Gaudet. 2015. Effect of the DGAT1 inhibitor pradigastat on triglyceride and apoB48 levels in patients with familial chylomicronemia syndrome. *Lipids Health Dis.* **14**: 8.
36. Stephen, J., T. Vilboux, Y. Haberman, H. Pri-Chen, B. Pode-Shakked, S. Mazaheri, D. Marek-Yagel, O. Barel, A. Di Segni, E. Eyal, et al. 2016. Congenital protein losing enteropathy: an inborn error of lipid metabolism due to DGAT1 mutations. *Eur. J. Hum. Genet.* **24**: 1268–1273.
37. Ratchford, T. L., A. J. Kirby, H. Pinz, and D. R. Patel. Congenital diarrhea from DGAT1 mutation leading to electrolyte derangements, protein-losing enteropathy, and rickets. *J. Pediatr. Gastroenterol. Nutr.* **66**: e82–e83.
38. Chen, H. C., S. J. Stone, P. Zhou, K. K. Buhman, and R. V. Farese, Jr. 2002. Dissociation of obesity and impaired glucose disposal in mice overexpressing acyl coenzyme A: diacylglycerol acyltransferase 1 in white adipose tissue. *Diabetes*. **51**: 3189–3195.
39. Koliwad, S. K., R. S. Streeter, M. Monetti, I. Cornelissen, L. Chan, K. Terayama, S. Naylor, M. Rao, B. Hubbard, and R. V. Farese, Jr. 2010. DGAT1-dependent triacylglycerol storage by macrophages protects mice from diet-induced insulin resistance and inflammation. *J. Clin. Invest.* **120**: 756–767.
40. Liu, L., X. J. Shi, K. G. Bharadwaj, S. Ikeda, H. Yamashita, H. Yagyu, J. E. Schaffer, Y. H. Yu, and I. J. Goldberg. 2009. DGAT1 expression increases heart triglyceride content but ameliorates lipotoxicity. *J. Biol. Chem.* **284**: 36312–36323.
41. Buhman, K. K., S. J. Smith, S. J. Stone, J. J. Repa, J. S. Wong, F. F. Knapp, Jr., B. J. Burri, R. L. Hamilton, N. A. Abumrad, and R. V. Farese, Jr. 2002. DGAT1 is not essential for intestinal triacylglycerol absorption or chylomicron synthesis. *J. Biol. Chem.* **277**: 25474–25479.
42. Cheng, D., J. Iqbal, J. Devenny, C. H. Chu, L. Chen, J. Dong, R. Seethala, W. J. Keim, A. V. Azzara, R. M. Lawrence, et al. 2008. Acylation of acylglycerols by acyl coenzyme A: diacylglycerol acyltransferase 1 (DGAT1): functional importance of DGAT1 in the intestinal fat absorption. *J. Biol. Chem.* **283**: 29802–29811.
43. Hong, Y. B., J. Kang, J. H. Kim, J. Lee, G. Kwak, Y. S. Hyun, S. H. Nam, H. D. Hong, Y. R. Choi, S. C. Jung, et al. 2016. DGAT2 mutation in a family with autosomal-dominant early-onset axonal Charcot-Marie-Tooth disease. *Hum. Mutat.* **37**: 473–480.
44. Smith, S. J., S. Cases, D. R. Jensen, H. C. Chen, E. Sande, B. Tow, D. A. Sanan, J. Raber, R. H. Eckel, and R. V. Farese, Jr. 2000. Obesity resistance and multiple mechanisms of triglyceride synthesis in mice lacking Dgat. *Nat. Genet.* **25**: 87–90.
45. Cardell, R. R., S. Badenhausen, and K. R. Porter. 1967. Intestinal triglyceride absorption in the rat. An electron microscopical study. *J. Cell Biol.* **34**: 123–155.
46. D'Aquila, T., Y. H. Hung, A. Carreiro, and K. K. Buhman. 2016. Recent discoveries on absorption of dietary fat: Presence, synthesis, and metabolism of cytoplasmic lipid droplets within enterocytes. *Biochim. Biophys. Acta*. **1861** (8 Pt A): 730–747.
47. Yen, C. L., S. J. Stone, S. Koliwad, C. Harris, and R. V. Farese, Jr. 2008. DGAT enzymes and triacylglycerol biosynthesis. *J. Lipid Res.* **49**: 2283–2301.
48. Kaser, A., A. H. Lee, A. Franke, J. N. Glickman, S. Zeissig, H. Tilg, E. E. Nieuwenhuis, D. E. Higgins, S. Schreiber, L. H. Glimcher, et al. 2008. XBP1 links ER stress to intestinal inflammation and confers genetic risk for human inflammatory bowel disease. *Cell*. **134**: 743–756.
49. Beyaz, S., M. D. Mana, J. Roper, D. Kedrin, A. Saadatpour, S. J. Hong, K. E. Bauer-Rowe, M. E. Xifaras, A. Akkad, E. Arias, et al. 2016. High-fat diet enhances stemness and tumorigenicity of intestinal progenitors. *Nature*. **531**: 53–58.
50. Han, J., and R. J. Kaufman. 2016. The role of ER stress in lipid metabolism and lipotoxicity. *J. Lipid Res.* **57**: 1329–1338.